SIMONA Flight Simulator Implementation of a Fault Tolerant Sliding Mode Scheme with On–line Control Allocation

H. Alwi, C. Edwards, O. Stroosma and J.A. Mulder

Abstract— **This paper considers a sliding mode based allocation scheme for fault tolerant control. The scheme allows redistribution of the control signals to the remaining functioning actuators when a fault or failure occurs. It is shown that faults and even certain total actuator failures can be handled directly without reconfiguring the controller. The results obtained from implementing the controller on the SIMONA flight motion simulator show good performance in both nominal and failure scenarios even in wind and gust conditions.**

I. INTRODUCTION

Incidents such as the DHL flight, Baghdad, Nov. 2003 (which was hit by a missile on its left wing and lost all hydraulics, but still landed safely without any casualties) represent examples of successful landings using clever manipulation of the throttle levers, that has motivated research into fault tolerant control (FTC). Control allocation (CA) has emerged as one potential technique for dealing with systems with redundancy such as large transport aircraft. Researchers like [6], [2] have shown the capabilities of CA for systems with faults and failures. One of the benefits of CA is that the controller structure does not have to be reconfigured in the case of faults and it can deal directly with total actuator failures without requiring reconfiguration of the controller, because the CA scheme 'automatically' redistributes the control signal.

The insensitivity and robustness properties of sliding mode control to certain types of disturbances and uncertainty [7], especially to actuator faults, make it attractive for FTC especially in the area of flight control. Sliding modes cannot deal directly with actuator failures. However control allocation provides a solution to this problem by providing access to the 'redundant' actuators. Therefore, a combination of sliding mode and control allocation provides a powerful tool for the development of simple, robust fault tolerant flight controllers that work for a wide range of faults and failures. The work in [14], [18] provides practical examples of the combination of sliding mode control (SMC) and CA for FTC. The work by Shin *et al.*[13] uses control allocation ideas, but formulates the problem from an adaptive controller point of view. However none of these papers provide a detailed stability analysis and discuss sliding mode controller design issues when using control allocation. More recently in [1], a sliding mode control

allocation scheme was proposed for a more general class of uncertain linear systems. A set of easily testable conditions was developed to guarantee the stability of the closed–loop system subject to a class of actuator faults. The scheme in [1] uses a control law which depends on (an estimate of) the 'efficiency/effectiveness' of the actuators. This paper presents the 'piloted' results obtained from implementing the ideas from [1] tested on an advanced 6 degree of freedom (6–DOF) research flight simulator called SIMONA (SImulation, MOtion and NAvigation).

II. THE SIMONA RESEARCH SIMULATOR

The SIMONA (SImulation, MOtion and NAvigation) Research Simulator (SRS) in Figure 1 is a research project of the Delft University of Technology. The SRS provides researchers with a powerful tool that can be adapted to various uses [16]. In the years since it has been operational, the SRS has been used for research into human (motion) perception [11], aircraft handling qualities [9],fly-by-wire control algorithms and flight deck displays [12] and flight procedures [8]. The flexible software architecture and high-fidelity cueing environment allows the integration of the B747 model from [15], complete with failures and the assessment of the controller in a realistic aircraft environment.
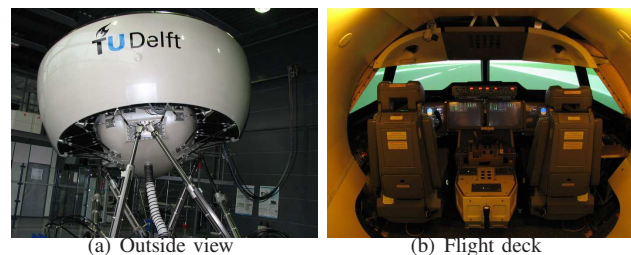

(a) Outside view   (b) Flight deck

Fig. 1. SIMONA research simulator

The flight deck of the SRS (Figure1(b)) provides the pilots with simulated instruments that match the aircraft under investigation. The pilots interface with the aircraft by a conventional control column or a sidestick controller, rudder pedals with engine controls and a Mode Control Panel (MCP) for the autopilot. The windows give a wide view on a virtual environment and a motion system moves the entire cabin to simulate aircraft motion cues.

A modular network of personal computers (PCs) provides the processing power to run the simulator. Each PC has a specific task, e.g. driving the pilot controls, generating the instrument display graphics, running the aircraft model or logging data. A high-speed fibre-optic network provides synchronization and communication services for all the

H. Alwi and C. Edwards are with Control and Instrumentation Research Group, Department of Engineering, University of Leicester, University Road, Leicester LE1 7RH, UK. O. Stroosma is with International Research Institute for Simulation, Motion and Navigation (SIMONA), P.O. BOX 5058, 2600 GB Delft, The Netherlands. J.A. Mulder is with Control and Simulation Division, Faculty of Aerospace Engineering, Delft University of Technology, 2600 GB Delft, The Netherlands.

computers. The modular approach makes it easy to exchange for example the aircraft model for another, without affecting the rest of the simulation software. In particular, the software is able to interface with MATLAB SIMULINK models.

The FTLAB747 software running under MATLAB has been developed for the study of fault tolerant control and FDI schemes. It represents a 'real world' model of a B747-100/200 aircraft. More recently this software has been upgraded to V6.5/7.1/2006b by Smaili *et al.*[15] as part of the GARTEUR AG16, to allow all the control surfaces to be controlled independently offering more degrees of control flexibility especially during faults or failures. This 'modified' aircraft is essentially a fly by wire aircraft [3] where all the control surfaces are controlled electronically compared to the 'classical' B747 aircraft. To be able to fly with a pilot in the loop in SRS, the benchmark B747 model [15] was slightly adapted from the offline model. The aircraft model was isolated from peripheral utility functions such as the autopilot, to follow the reference scenario and MATLAB logging functions. Its inputs and outputs were standardized to fit in the SRS software environment and the SIMULINK model was converted to C code using the Real-Time Workshop. Finally the model was integrated with the pilot controls, aircraft instruments and cueing devices of the SRS.

III. A SLIDING MODE CONTROL ALLOCATION SCHEME

It will be assumed that the system subject to actuator faults or failures, can be written as

$$\dot{x}(t) = Ax(t) + Bu(t) - BK(t)u(t) \tag{1}$$

where $A \in \mathbb{R}^{n \times n}$ and $B \in \mathbb{R}^{n \times m}$. The effectiveness gain $K(t) = \text{diag}(k_1(t), \ldots, k_m(t))$ where the $k_i(t)$ are scalars satisfying $0 \le k_i(t) \le 1$. These scalars model a decrease in effectiveness of a particular actuator. If $k_i(t) = 0$, the ith actuator is working perfectly whereas if $k_i(t) > 0$, a fault is present, and if $k_i(t) = 1$ the actuator has failed completely. For most systems with actuator redundancy, the assumption that $\text{rank}(B) = l < m$, often employed in the literature, is not valid. However, the system states can be reordered, and the matrix B from (1) can be partitioned as:

$$B = \begin{bmatrix} B_1 \\ B_2 \end{bmatrix} \tag{2}$$

where $B_1 \in \mathbb{R}^{(n-l) \times m}$ and $B_2 \in \mathbb{R}^{l \times m}$ has rank l. In aircraft systems, B_2 is associated with the equations of angular acceleration in roll, pitch and yaw [10]. Here it is assumed that the matrix B_2 represents the dominant contribution of the control action on the system, while B_1 generally will have elements of small magnitude compared with $\|B_2\|$. Compared to the work in [13] where it is assumed that $B_1 = 0$, here $B_1 \ne 0$ will be considered explicitly in the controller design and in the stability analysis. It will be assumed without loss of generality that the states of the system in (1) have been transformed so that $B_2 B_2^T = I_l$ and therefore $\|B_2\| = 1$. As in [1], let the 'virtual control'

$\nu(t)$ be defined as $\nu(t) := B_2 u(t)$ so that $u(t) = B_2^\dagger \nu(t)$ where the pseudo inverse is chosen as

$$B_2^\dagger := W B_2^T (B_2 W B_2^T)^{-1} \tag{3}$$

and $W \in \mathbb{R}^{m \times m}$ is a symmetric positive definite (s.p.d) diagonal weighting matrix. As in [1], in this paper, a novel choice of weighting matrix W will be considered. Specifically, the weight W has been chosen as

$$W := I - K \tag{4}$$

and so $W = \text{diag}\{w_1, \ldots, w_m\}$ where $w_i = 1 - k_i$. As argued in [1], as $k_i \to 1$, the signal u_i sent to the ith actuator tends to zero.

In [1], sliding mode control (SMC) techniques [7], have been used to synthesize the 'virtual control' $\nu(t)$. Define a switching function $\sigma(t) : \mathbb{R}^n \to \mathbb{R}^l$ to be

$$\sigma(t) = Sx(t)$$

where $S \in \mathbb{R}^{l \times n}$ and $\det(SB_\nu) \ne 0$. Let $\mathcal{S}$ be the hyperplane defined by $\mathcal{S} = \{x(t) \in \mathbb{R}^n : Sx(t) = 0\}$. If a control law can be developed which forces the closed–loop trajectories onto the surface $\mathcal{S}$ in finite time and constrains the states to remain there, then an ideal sliding motion is said to have been attained [7]. Define

$$\hat{\nu}(t) := (B_2 W^2 B_2^T)(B_2 W B_2^T)^{-1} \nu(t) \tag{5}$$

then as argued in [1], after an appropriate coordinate transformation, $x \mapsto T_r x = \hat{x}$, equation (1) becomes:

$$\begin{bmatrix} \dot{\hat{x}}_1(t) \\ \dot{\hat{x}}_2(t) \end{bmatrix} = \underbrace{\begin{bmatrix} \hat{A}_{11} & \hat{A}_{12} \\ \hat{A}_{21} & \hat{A}_{22} \end{bmatrix}}_{\hat{A}} \begin{bmatrix} \hat{x}_1(t) \\ \hat{x}_2(t) \end{bmatrix} + \underbrace{\begin{bmatrix} 0 \\ I \end{bmatrix}}_{\hat{B}} \hat{\nu}(t) + \begin{bmatrix} B_1 B_2^N B_2^+ \\ 0 \end{bmatrix} \hat{\nu}(t) \tag{6}$$

where

$$B_2^+ := W^2 B_2^T (B_2 W^2 B_2^T)^{-1} \tag{7}$$

and

$$B_2^N := (I - B_2^T B_2) \tag{8}$$

then there is an upper bound on the norm of the pseudo-inverse B_2^+ in (7) which is independent of W. Specifically:

Proposition 1: There exists a scalar γ_0 which is finite and independent of W such that

$$\|B_2^+\| = \|W^2 B_2^T (B_2 W^2 B_2^T)^{-1}\| < \gamma_0 \tag{9}$$

for all $W = diag(w_1 \ldots w_m)$ such that $0 < w_i \le 1$.
Proof: see [1]. ∎

The virtual control law $\hat{\nu}(t)$ will now be designed based on the fault-free system in which the last term in (6) is zero since $B_1 B_2^N B_2^+|_{W=I} = 0$. In the $\hat{x}(t)$ coordinates in (6), a choice for the sliding surface is

$$\hat{S} := S T_r^{-1} = \begin{bmatrix} M & I_l \end{bmatrix} \tag{10}$$

where $M \in \mathbb{R}^{l \times (n-l)}$ represents design freedom. Define

$$\gamma_1 := \|M B_1 B_2^N\| \tag{11}$$

If $(\hat{A}, \hat{B})$ is controllable, then $(\hat{A}_{11}, \hat{A}_{12})$ is controllable [7] and a matrix M can always be found to make the matrix $\tilde{A}_{11} = \hat{A}_{11} - \hat{A}_{12}M$ stable. Define

$$\tilde{G}(s) := \tilde{A}_{21}(sI - \tilde{A}_{11})^{-1}B_1 B_2^N \tag{12}$$

where s represents the Laplace variable and the matrix $\tilde{A}_{21} := M\hat{A}_{11} + \hat{A}_{21} - \hat{A}_{22}M$. By construction the transfer function $\tilde{G}(s)$ is stable. If

$$\|\tilde{G}(s)\|_\infty = \gamma_2 \tag{13}$$

then the following is true:

Proposition 2: During a fault or failure condition, for any combinations of $0 < w_i \le 1$, the closed–loop system will be stable if

$$0 < \frac{\gamma_2 \gamma_0}{1 - \gamma_1 \gamma_0} < 1 \tag{14}$$

Proof: see [1]. ∎

The proposed control law from [1] has a structure given by $\hat{\nu}(t) = \hat{\nu}_l(t) + \hat{\nu}_n(t)$ where

$$\hat{\nu}_l(t) := -\tilde{A}_{21}\hat{x}_1(t) - \tilde{A}_{22}\sigma(t) \tag{15}$$

where $\tilde{A}_{22} := M\hat{A}_{12} + \hat{A}_{22}$ and the nonlinear component is defined to be

$$\hat{\nu}_n(t) := -\rho(t, x)\frac{\sigma(t)}{\|\sigma(t)\|} \quad \text{for } \sigma(t) \neq 0 \tag{16}$$

where $\sigma(t) = \hat{S}\hat{x}(t)$.

Proposition 3: Suppose the hyperplane matrix M has been chosen so that $\tilde{A}_{11} = \hat{A}_{11} - \hat{A}_{12}M$ is stable and condition (14) from Proposition 2 holds, then choosing

$$\rho(t, x) := \frac{\gamma_1 \gamma_0 \|\hat{\nu}_l(t)\| + \eta}{1 - \gamma_1 \gamma_0} \tag{17}$$

ensures a sliding motion takes place on $\mathcal{S}$ in finite time.
Proof: see [1]. ∎

The control law is finally given as

$$u(t) = WB_2^{\mathrm{T}}(B_2 W^2 B_2^{\mathrm{T}})^{-1}\hat{\nu}(t) \tag{18}$$

IV. CONTROLLER DESIGN

In this paper both lateral and longitudinal control is considered. One of the controller design objectives considered here is to bring a faulty aircraft to a near landing condition. This can be achieved by a change of direction through a 'banking turn' manoeuvre [4], followed by a decrease in altitude and speed. This can be achieved by tracking appropriate roll angle (ϕ) and sideslip angle (β) commands using the lateral controller, and tracking flight path angle (FPA) and airspeed (V_{tas}) commands using the longitudinal controller. A linearization has been obtained around an operating condition of 263,000 Kg, 92.6 m/s true airspeed, and an altitude of 600m at 25.6% of maximum thrust and at a 20deg flap position. The lateral control surfaces are $\delta_{lat} = [\delta_{air}\ \delta_{ail}\ \delta_{aor}\ \delta_{aol}\ \delta_{sp1-4}\ \delta_{sp5}\ \delta_8\ \delta_{sp9-12}\ e_{lat1-4}]^{\mathrm{T}}$ which represent aileron deflection (right & left - inner & outer)(rad), spoiler deflections (left: 1-4 & 5 & right: 7 & 9-12) (rad), rudder deflection (rad) and lateral engine (1-4) pressure ratios (EPR). The longitudinal control surfaces

are $\delta_{long} = [\delta_e\ \delta_s\ e_{long1-4}]^{\mathrm{T}}$ which represent elevator deflection (rad), horizontal stabilizer deflection (rad), and longitudinal (engine 1-4) EPR. To include a tracking facility, integral action [7], [1] has been included for both longitudinal and lateral control.

A. Lateral Controller Design

It can be verified from a numerical search that $\gamma_{0_{lat}}$ from (9) is $\gamma_{0_{lat}} = 8.1314$. The matrix which defines the hyperplane must now be synthesized so that the conditions of (14) are satisfied. A quadratic optimal design has been used to obtain the sliding surface $S_{a_{lat}}$ which depends on the matrix M_{lat} in equation (10) (see for example [17], [7]) where the symmetric positive definite state weighting matrix has been chosen as $Q_{lat} = diag(0.005, 0.1, 6, 6, 1, 1)$. The first two terms of Q_{lat} are associated with the integral action and are less heavily weighted. The third and fourth term of Q_{lat} are associated with the equations of the angular acceleration in roll and yaw (i.e. $B_{lat,2}$ term partition in (2)) and thus weight the virtual control term. Thus by analogy to a more typical LQR framework, they affect the speed of response of the closed–loop system. Here, the third and fourth terms of Q_{lat} have been heavily weighted compared to the last two terms to reflect a reasonably fast closed–loop system response. The poles associated with the reduced order sliding motion are $\{-0.0707, -0.3867, -0.3405 \pm 0.1484i\}$. Based on this value of M_{lat}, simple calculations from (11) show that $\gamma_{1_{lat}} = 0.0145$, therefore $\gamma_{0_{lat}}\gamma_{1_{lat}} = 0.1180 < 1$ and so the requirements of (14) are satisfied. Also for this choice of sliding surface, $\|\tilde{G}_{lat}(\mathsf{s})\|_\infty = \gamma_{2_{lat}} = 0.0764$ from (13). Therefore from (14),

$$\frac{\gamma_{2_{lat}}\gamma_{0_{lat}}}{1 - \gamma_{1_{lat}}\gamma_{0_{lat}}} = 0.7043 < 1$$

which shows that the system is stable for all choices of $0 < w_i \le 1$. The nonlinear gain $\rho_{lat} = 1$ from (16) have been chosen. For implementation, the discontinuity in the nonlinear control term in (16) has been smoothed by using a sigmoidal approximation where the scalar $\delta_{lat} = 0.05$ (see for example §3.7 in [7]).

To emulate a real aircraft flight control capability, an outer loop heading control was designed based on a proportional controller plus washout filter, to provide a roll command to the inner loop sliding mode controller. In the SIMONA implementation, this outer loop heading control can be activated by a switch in the cockpit. The proportional gain was set as $K_{p_{lat}} = 0.5$ and the washout filter $\frac{s}{s+5}$ was assigned a gain $K_{wf_{lat}} = 0.1$.

B. Longitudinal Controller Design

It can be verified from a numerical search that $\gamma_{0_{long}} = 8.2913$ from (9). As in the lateral controller, a quadratic optimal design has been used to obtain the sliding surface matrix (and therefore the matrix M_{long}). The s.p.d weighting matrix has been chosen as $Q_{long} = diag(0.1, 0.1, 10, 50, 1, 1)$. The third and fourth terms of Q_{long} are associated with the $B_{long,2}$ term partition in (2) (i.e. states q and V_{tas}) which weight the virtual control term,

and have been heavily weighted compared to the last two terms. The poles associated with the reduced order sliding motion are $\{-0.7066, -0.2393 \pm 0.1706i, -0.0447\}$. Based on this value of M_{long}, simple calculations from (11) show that $\gamma_{1_{long}} = 1.9513 \times 10^{-4}$: therefore $\gamma_{0_{long}} \gamma_{1_{long}} = 0.0016 < 1$ and so the requirements of equation (14) are satisfied. For this choice of sliding surface, $\|\tilde{G}_{long}(\mathbf{s})\|_\infty = \gamma_{2_{long}} = 0.0112$ from (13). Therefore from (14),

$$\frac{\gamma_{2_{long}} \gamma_{0_{long}}}{1 - \gamma_{1_{long}} \gamma_{0_{long}}} = 0.0931 < 1$$

which shows that the system is stable for all choices of $0 < w_i \le 1$. The nonlinear gain $\rho_{long} = 1$ from (16) have been chosen. The discontinuity in the nonlinear control term in (16) has been smoothed by using a sigmoidal approximation where the scalar $\delta_{long} = 0.05$.

An outer loop altitude control scheme was designed based on a proportional controller plus washout filter to provide a FPA command to the inner loop sliding mode controller. In the SIMONA implementation, this outer loop altitude control can be activated by a switch in the cockpit. The proportional gain was set as $K_{p_{long}} = 0.001$ and the washout filter $\frac{s}{s+5}$ with the gain $K_{wf_{long}} = 0.05$.

Note that both the lateral and longitudinal controller manipulate the engine EPRs. In the trials, 'control mixing' was employed, where the individual EPR signals from both the lateral controller and longitudinal controller were added together before being applied into each of the engines. This is similar to the control strategy used for the NASA propulsion control aircraft described in [5].

V. SIMONA IMPLEMENTATIONS

The controller was implemented as a MATLAB SIMULINK (version 2006b) model with appropriate inputs and outputs to connect it with the aircraft model and the SIMONA hardware, as described in Figure 2. All data is time stamped, ensuring consistency across different modules within the simulation, even when they are on physically different processors. The controller was set up to work with an Ode2
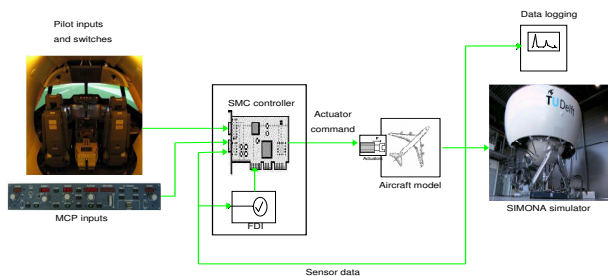

Fig. 2. SIMONA interconnections

(Heun) solver with a fixed time step of 0.01 s (100 Hz). Using the Real-Time Workshop, the SIMULINK controller block diagram was converted to C-code and integrated into the SRS, where it runs on a dual Pentium III 1 GHz processor, together with the aircraft model and motion control software. A connection with the Mode Control Panel on the flight deck enables the selection of 'control modes'

e.g. altitude hold, heading select and reference values. The simulator trials were performed with the speed, altitude and heading select modes active. The pilot commands new headings, speeds or altitudes by adjusting the controls on the MCP. In this paper, it will be assumed that a measurement of the actual actuator deflection is available. This is not an unrealistic assumption in aircraft systems [3]. Information provided by the actual actuator deflection can be compared with the signals from the controller to indicate the effectiveness of the actuator.

VI. RESULTS

The results presented in this paper are all from the 6–DOF SIMONA research simulator trials. It was assumed that the aircraft has recently taken off and reached an altitude of 600m. After a few seconds of straight and level flight, failures occur on the actuators. The immediate action requested by the pilot is to change the heading to 180deg and to head back to the runway. The altitude is then changed from 600m (1967.2ft) to 30.5m (100ft) before the V_{tas} is reduced from 92.8m/s(180kn) to 82.3m/s(160kn), to approximate a landing manoeuvre.

Five different control surface failures have been tested on the simulator: all elevators jam with a 3deg offset; all ailerons jam with a 3deg offset; a stabilizer runaway; all rudders runaway and finally both rudders detach from the vertical fin [15]. All the trials have been done with and without wind and turbulence. However due to space limitations, only the most significant results are shown.

Figure 3 shows the fault–free responses. The heading is changed by means of two 90deg step inputs followed by a change in altitude from 600m to 30m in 3 steps: 600m to 366m to 183m and finally to 30m above the runway.

Figures 4-6 show a stabilizer runaway failure. Figure 5 shows that the stabilizer has moved at its maximum deflection rate to its maximum deflection of 3deg. This is quite a catastrophic failure as this deflection causes the aircraft to pitch down, if not corrected. Figure 4 shows no visible degradation in performance. Figure 6 shows that the effectiveness of the stabilizer has been successfully estimated and this information has been used to provide on–line control allocation.

Figures 7 -9 show the system responses when the upper and lower rudder detaches from the vertical fin in the presence of wind and gusts. This is shown clearly in figure 8 where at the start of the simulation, the rudder moves due to wind and gust, and when the rudders are detached, there is no longer any deflection detected by the sensor. Figure 7 shows that without the rudders, the aircraft manages to maintain a slightly degraded level of performance even in more challenging wind and gust conditions. There is visually no difference in the sideslip performance compared to the nominal situation in figure 3. Figure 8 shows that the differential EPR has been successfully used to maintain sideslip tracking during the heading change.

Figures 10-12 show the responses for a rudder runaway. Figure 11 shows that the upper and lower rudders runaway

to the 5deg position. This is the hardest situation to control. Not only does the rudder runaway cause a tendency to turn to one side (and therefore affecting lateral control performance), it also creates difficulties in the longitudinal axis and results in a tendency to pitch up. Figure 10 shows that the controller is tested on a slightly different manoeuvre. The sideslip command is kept at 0deg and has only small degradation in its performance. The heading is changed by 180deg by banking to the right and at the same time the speed is increased to 113.18m/s (220kn) adding further difficulties to the banking manoeuvre. Then a bank left is tested by changing the demanded heading back to 135deg, followed by a reduction in speed to 92.6m/s. The altitude is also decreased to 30m, before a small increase in altitude to 182m above the runway. In these tests, only a small degradation in performance is visible. Figure 12 shows that the switching function just exceeds the threshold at high speed indicating that at higher speed, the effect of the rudder runaway is harder to control. However, using the rudder effectiveness information in figure 12 the control signal sent to the rudder is shut–off and the control signals are sent to the remaining functioning actuators causing a visible split in the control surface deflections seen in figure 11. Figure 11 shows the 4 engine pressure ratios (EPR) have split to counteract the effect of the banking turn to the left. Engine 3 (red line) and 4 (green line) on the right wing show less EPR compared to Engine 1 (red line) and 2 (green line) on the left wing to counteract the tendency to turn to the left. The spoilers and ailerons also show a visible split in terms of the deflections to counteract the rudder runaway.

VII. Conclusions

This paper has presented a sliding mode control allocation scheme for fault tolerant control. The control allocation aspect is used to allow the sliding mode controller to redistribute the control signals to the remaining functioning actuators when a fault or failure occurs, without reconfiguring or switching to another controller. The scheme has been implemented on the SIMONA research flight simulator and has shown good performance not only in nominal conditions, but also in the case of total actuator failures, even in wind and gust conditions.

References

[1] H. Alwi and C. Edwards. Sliding mode FTC with on–line control allocation. In *45th IEEE Conference on Decision and Control*, 2006.
[2] J.D. Boskovic and R.K. Mehra. Control allocation in overactuated aircraft under position and rate limiting. In *Proceedings of the American Control Conference*, pages 791–796, 2002.
[3] D. Brière and P. Traverse. Airbus A320/A330/A340 electrical flight controls: A family of fault-tolerant systems. *Digest of Papers FTCS-23 The Twenty-Third International Symposium on Fault-Tolerant Computing*, pages 616–623, 1993.
[4] A. E. Bryson. *Control of spacecraft and aircraft*. Princeton University Press, 1994.
[5] F. W. Burcham, T. A. Maine, J. Kaneshinge, and J. Bull. Simulator evaluation of simplified propulsion–only emergency flight control system on transport aircraft. Technical Report NASA/TM-1999-206578, NASA, 1999.

[6] J.B. Davidson, F.J. Lallman, and W.T. Bundick. Real-time adaptive control allocation applied to a high performance aircraft. In *5th SIAM Conference on Control & Its Application*, 2001.
[7] C. Edwards and S.K. Spurgeon. *Sliding Mode Control: Theory and Applications*. Taylor & Francis, 1998.
[8] W.F. De Gaay Fortman, M.M. Van Paassen, M. Mulder, A.C. In't Veld, and J.-P. Clarke. Implementing time-based spacing for decelerating approaches. *Journal of Aircraft*, 44:106–118, 2007.
[9] B. Gouverneur, J.A. (Bob) Mulder, M.M (René) van Paassen, and O. Stroosma. Optimization of the simona research simulator's motion filter settings for handling qualities experiments. In *AIAA Modeling and Simulation Technologies Conference and Exhibit*, 2003.
[10] O. Härkegård and S. T. Glad. Resolving actuator redundancy - optimal control vs. control allocation. *Automatica*, 41:137–144, 2005.
[11] H.M Heerspink, W.R. Berkouwer, O. Stroosma, M.M van Paassen, M. Mulder, and J.A. Mulder. Evaluation of vestibular thresholds for motion detection in the simona research simulator. In *AIAA Modeling and Simulation Technologies Conference*, 2005.
[12] T.M. Lam, M. Mulder, M.M. Van Paassen, and J.A. Mulder. Comparison of control and display augmentation for perspective flight-path displays. *Journal of Guidance, Control, and Dynamics*, 29:564–578, 2006.
[13] D. Shin, G. Moon, and Y. Kim. Design of reconfigurable flight control system using adaptive sliding mode control: actuator fault. *Proceedings of the Institution of Mechanical Engineers, Part G (Journal of Aerospace Engineering)*, 219:321–328, 2005.
[14] Y. Shtessel, J. Buffington, and S. Banda. Tailless aircraft flight control using multiple time scale re-configurable sliding modes. *IEEE Transactions on Control Systems Technology*, 10:288–296, 2002.
[15] M.H. Smaili, J. Breeman, T.J.J. Lombaerts, and D.A. Joosten. A simulation benchmark for integrated fault tolerant flight control evaluation. In *AIAA Modeling and Simulation Technologies Conference and Exhibit*, 2006.
[16] O. Stroosma, M.M van Paassen, and M. Mulder. Using the simona research simulator for human-machine interaction research. In *AIAA Modeling and Simulation Technologies Conference*, 2003.
[17] V.I. Utkin. *Sliding Modes in Control Optimization*. Springer-Verlag, Berlin, 1992.
[18] S.R. Wells and R.A. Hess. Multi–input/multi–output sliding mode control for a tailless fighter aircraft. *Journal of Guidance, Control and Dynamics*, 26:463–473, 2003.
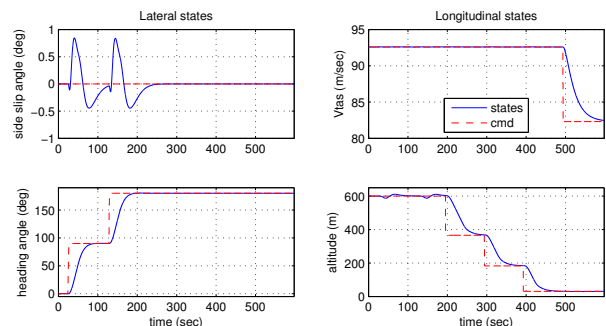
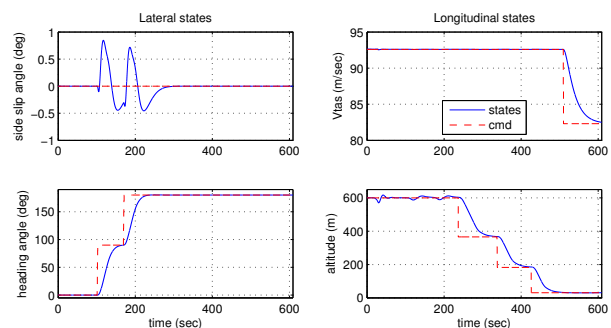Fig. 3. no fault condition: controlled states

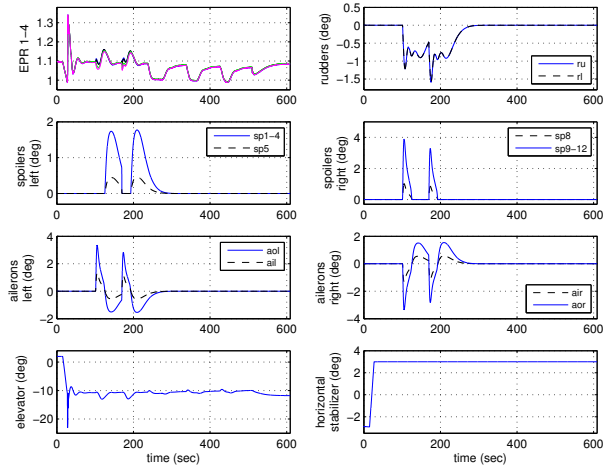Fig. 4. stabilizer runaway, FDI on: controlled states

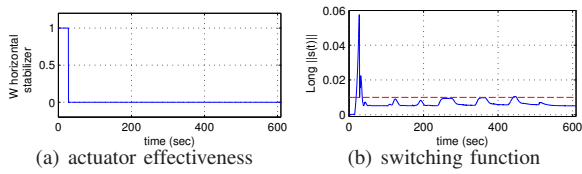Fig. 5.   stabilizer runaway, FDI on: actuator positions

Fig. 6.   stabilizer runaway, FDI on
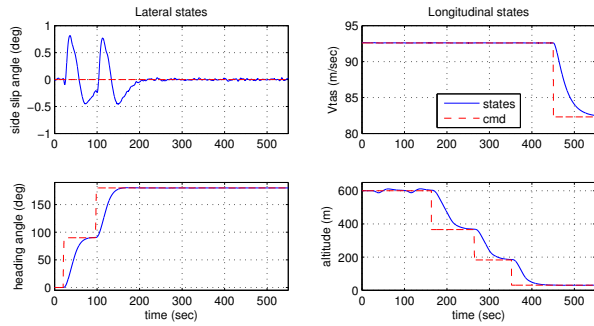

Fig. 7.   rudder missing with wind & gust, FDI on: controlled states
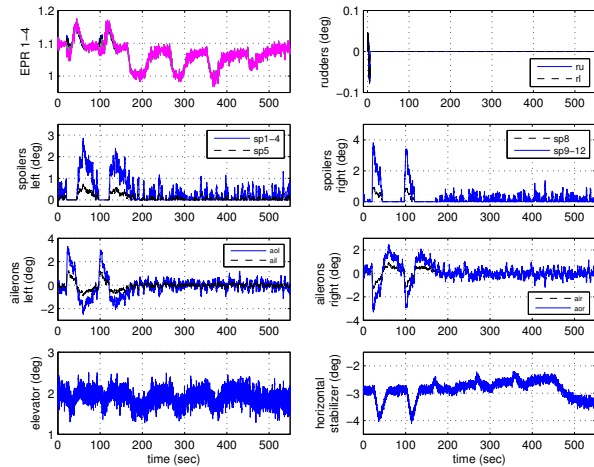

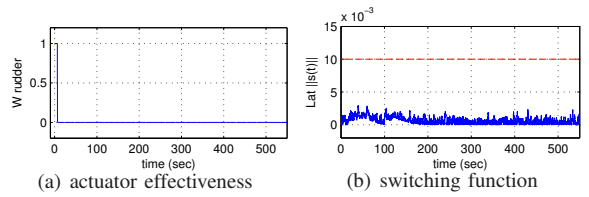Fig. 8.   rudder missing with wind & gust, FDI on: actuator positions

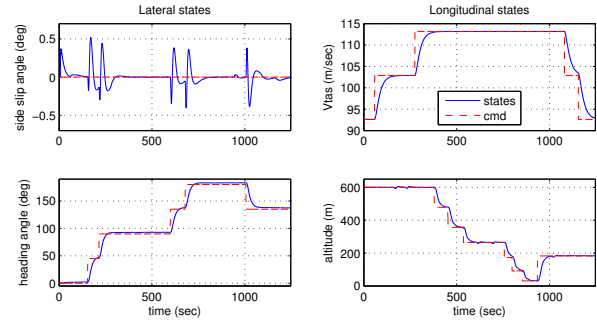Fig. 9.   rudder missing, FDI on

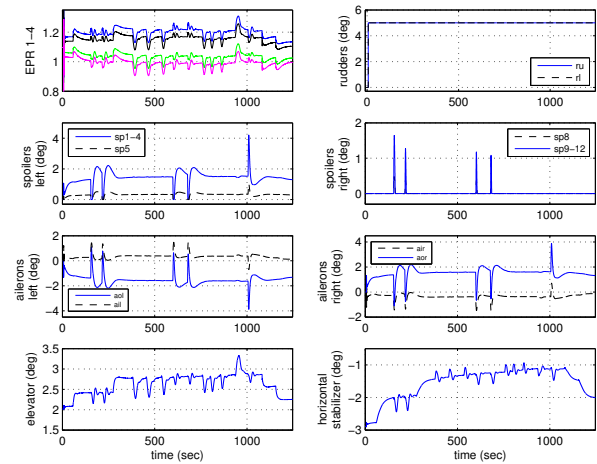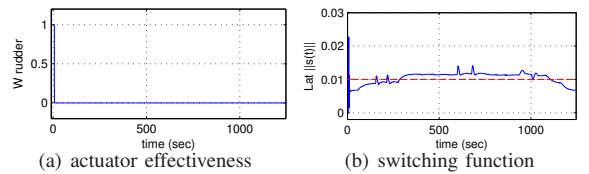Fig. 10.   rudder runaway, FDI on: controlled states

Fig. 11.   rudder runaway, FDI on: actuator positions

Fig. 12.   rudder runaway, FDI on